



1 **A large sample analysis of seasonal river flow correlation and its physical**
2 **drivers**

3 Theano Iliopoulou^{1*}, Cristina Aguilar², Berit Arheimer³, María Bermúdez⁴, Nejc Bezak⁵, Andrea
4 Ficchi⁶, Demetris Koutsoyiannis¹, Juraj Parajka⁷, María José Polo², Guillaume Thirel⁸ and Alberto
5 Montanari⁹

6 ⁽¹⁾ Department of Water Resources and Environmental Engineering, School of Civil Engineering,
7 National Technical University of Athens, Zographou, 15780, Greece

8 ⁽²⁾ Fluvial dynamics and hydrology research group, Andalusian Institute of Earth System Research,
9 University of Cordoba, Cordoba, 14071, Spain

10 ⁽³⁾ Swedish Meteorological and Hydrological Institute, 601 76 Norrköping, Sweden

11 ⁽⁴⁾ Water and Environmental Engineering Group, Department of Civil Engineering, Universidade
12 da Coruña, 15071 A Coruña, , Spain

13 ⁽⁵⁾ Faculty of Civil and Geodetic Engineering, University of Ljubljana, Jamova 2, SI-1000
14 Ljubljana, Slovenia

15 ⁽⁶⁾ Department of Geography and Environmental Science, University of Reading, Reading, RG6
16 6AB, United Kingdom; formerly, IRSTEA, Hydrology Research Group (HYCAR), F-92761,
17 Antony, France

18 ⁽⁷⁾ Vienna University of Technology, Institute of Hydraulic Engineering and Water Resources
19 Management, Karlsplatz 13/222, A-1040 Vienna, Austria

20 ⁽⁸⁾ IRSTEA, Hydrology Research Group (HYCAR), F-92761, Antony, France

21 ⁽⁹⁾ Department DICAM, University of Bologna, Bologna, 40136, Italy

22 * *Correspondence to:* Theano Iliopoulou (anyily@central.ntua.gr)

23

24

25

26



27 **Abstract**

28 The geophysical and hydrological processes governing river flow formation exhibit persistence
29 at several timescales, which may manifest itself with the presence of positive seasonal
30 correlation of streamflow at several different time lags. We investigate here how persistence
31 propagates along subsequent seasons and affects low and high flows. We define the High Flow
32 Season (HFS) and the Low Flow Season (LFS) as the three-month and the one-month periods
33 which usually exhibit the higher and lower river flows, respectively. A dataset of 224 European
34 rivers spanning more than 50 years of daily flow data is exploited. We compute the lagged
35 seasonal correlation between selected river flow signatures, in HFS and LFS, and the average
36 river flow in the antecedent months. Signatures are peak and average river flow for HFS and
37 LFS, respectively. We investigate the links between seasonal streamflow correlation and various
38 physiographic catchment characteristics and hydro-climatic properties. We find persistence to be
39 more intense for LFS signatures than HFS. To exploit the seasonal correlation in flood frequency
40 estimation, we fit a bivariate Meta-Gaussian probability distribution to peak HFS flow and
41 average pre-HFS flow in order to condition the peak flow distribution in the HFS upon river flow
42 observations in the previous months. The benefit of the suggested methodology is demonstrated
43 by updating the flood frequency distribution one season in advance in real-world cases. Our
44 findings suggest that there is a traceable physical basis for river memory which in turn can be
45 statistically assimilated into flood frequency estimation to reduce uncertainty and improve
46 predictions for technical purposes.

47

48 **Keywords:** flood frequency, seasonal correlation, persistence, real-time flood forecasting, meta-
49 Gaussian



50 **1. Introduction**

51 Recent analyses for the Po River and the Danube River highlighted that catchments may exhibit significant
52 correlation between peak river flows and average flows in the previous months (Aguilar et al., 2017). Such
53 correlation is the result of the behaviours of the physical processes involved in the rainfall-runoff
54 transformation that may induce memory in river flows at several different time scales. The presence of long-
55 term persistence in streamflow has been known for a long time since the pioneering works of Hurst (1951)
56 and has been actively studied ever since (e.g. Koutsoyiannis, 2011; Montanari, 2012; O'Connell et al., 2016
57 and references therein). While a number of seasonal flow forecasting methods have been explored in the
58 literature (e.g. Bierkens and van Beek, 2009; Dijk et al., 2013), attempts to explicitly exploit streamflow
59 persistence in seasonal forecasting through information from past flows have been in general limited.
60 Koutsoyiannis et al. (2008) proposed a stochastic approach to incorporate persistence of past flows into a
61 prediction methodology for monthly average streamflow and found the method to outperform the historical
62 analogue method (see also Dimitriadis et al., 2016 for theory and applications of the latter) and artificial
63 neural network methods in the case of the Nile River. Similarly, Svensson (2016) assumed that the
64 standardized anomaly of the most recent month will not change during future months to derive monthly flow
65 forecasts for 1–3 months lead time and found the predictive skill to be superior to the analogue approach for
66 93 UK catchments. A few other studies have included past flow information in prediction schemes along
67 with teleconnections or other climatic indices (Piechota et al., 2001; Chiew et al., 2003; Wang et al., 2009).
68 Recently, it was shown that streamflow persistence, revealed as seasonal correlation, may also be relevant
69 for prediction of extreme events by allowing one to update the flood frequency distribution based on river
70 flow observations in the pre-flood season and reduce its bias and variability (Aguilar et al., 2017). The above
71 previous studies postulated that seasonal streamflow correlation may be due to the persistence of the
72 catchments storage and/or the weather, but no attempt was made to identify the physical drivers.

73 The present study aims to further inspect seasonal persistence in river flows and its determinants, by
74 referring to a large sample of catchments in 6 European countries (Austria, Sweden, Slovenia, France, Spain



75 and Italy). We focus on persistence properties of both high and low flows by investigating the following
76 research question: can floods and droughts be predicted, in probabilistic terms, by exploiting the information
77 provided by average flows in the previous months? The question is relevant for gaining a better
78 comprehension of catchment dynamics and planning mitigation strategies for natural hazards. In fact, we also
79 aim at determining what the physical conditions are, in terms of catchment properties, i.e. geology and
80 climate, which may induce seasonal persistence in river flow. To reach the latter goal, we identify a set of
81 descriptors for catchment behaviours and climate, and inspect their impact on correlation magnitude and
82 therefore predictability.

83 A few studies have analysed physical drivers of streamflow persistence on annual and deseasonalized
84 monthly and daily timeseries (Mudelsee, 2007; Hirpa et al., 2010; Gudmundsson et al., 2011; Zhang et al.,
85 2012; Szolgayova et al., 2014; Markonis et al., 2018) but the topic has been less studied on intra-annual scales
86 relevant to seasonal forecasting of floods and droughts.

87 Therefore, we herein follow up previous work by further investigating in a larger sample of catchments
88 the predictability of high and low flows in probabilistic terms. Additionally, we inspect the physical drivers
89 of correlation.

90

91 **2. Methodology**

92 The investigation of the persistence properties of river flows focuses separately on both high and low
93 discharges and is articulated in the following steps: (a) identification of the high- and low-flow seasons; (b)
94 correlation assessment between the peak flow in the high flow season (average flow in the low-flow season)
95 and average flows in the previous months; (c) analysis of the physical drivers for streamflow persistence and
96 its predictability through a Principal Component Analysis; (d) real-time updating of the flood frequency
97 distribution for selected case studies with significant seasonal correlation by employing a Meta-Gaussian
98 approach. The above steps are described in detail in the following sections.



99 **2.1 Season Identification**

100 Season identification is performed algorithmically to identify the High Flow Season (HFS) and Low Flow
101 Season (LFS) for each river time series. For the estimation of HFS, we employ an automated method recently
102 proposed by Lee et al. (2015), which identifies the high flow season as the three-month period centred around
103 the month with the maximum number of occurrences of Peaks Over Threshold (POT), with the threshold set
104 to the highest 5 % of the daily flows. To evaluate the selection of HFS, a metric constructed as the Percentage
105 of Annual Maximum Flows (PAMF) captured in the HFS is employed. The PAMFs are classified in
106 subjective categories of “poor” (<40 %), “low” (40–60 %), “medium” (60–80 %) and “high” (>80 %) values,
107 denoting the probability that the identified HFS is the dominant high-flow season in the record. If the
108 identified peak month alone contains 80 % or more of annual maxima flows, a uni-modal regime is assumed
109 and the identification procedure is terminated. In all other cases, the method allows for the search of a second
110 peak month and the identification of a minor HFS but we do not further elaborate on this analysis here because
111 we focus on the major HFS.

112 The method proposed by Lee et al. (2015) has several advantages that make it suitable for the purpose
113 of this research. Most importantly, it is capable of handling conditions of bi-modality, which is usually a
114 major issue for traditional methods like, e.g., directional statistics (Cunderlik et al., 2004). A potential
115 limitation is the assumption of symmetrical extension of HFS around the peak month, along with the uniform
116 selection of its length (3-month period). The degree of subjectivity in the evaluation of the second HFS is
117 another limitation, which is not relevant here as we focus on the main HFS.

118 LFS is herein identified as the one-month period with the lowest amount of mean monthly flow. An
119 alternative approach of estimating the relative frequencies of annual minima of monthly flow and selecting
120 the month with the highest frequency as LFS is also considered.

121 **2.2 Correlation analysis and physical interpretation through Principal Component Analysis**

122 In the case of HFS, a correlation is sought between the maximum daily flow occurring in the HFS period and
123 the mean flow in the previous months. For LFS, correlation is computed between the mean flow in the LFS



124 itself and the mean flow in the previous months. Since we are interested in seasonal persistence, we compute
125 the Pearson's correlation coefficient up to 9-month lag for HFS and 11-month lag for LFS.

126 An extensive investigation is carried out to identify physical drivers of seasonal streamflow correlation,
127 in terms of catchment, climatic and geological descriptors.

128 As catchment descriptors, we consider the basin area (A), the Baseflow Index (BI), the mean specific
129 runoff (SR) and the percentage of basin area covered by lakes (percentage of lakes, PL) and glaciers
130 (percentage of glaciers, PG) as candidate explanatory variables for streamflow correlation.

131 The area A (km^2) is primarily investigated as it is representative of the scale of the catchment, under
132 the assumption that in larger basins the impact of the climatological and geophysical processes affecting river
133 flow becomes more significant and may lead to a magnified seasonal correlation.

134 BI is considered basing on the assumption that high groundwater storage may be a potential driver of
135 correlation. BI is calculated from the daily flow series of the rivers following the hydrograph separation
136 procedure detailed in Gustard et al. (2009). Flow minima are sampled from non-overlapping 5-day blocks of
137 the daily flow series and turning points in the sequence of minima are sought and identified when the 90 %
138 value of a certain minimum is smaller or equal to its adjacent values. Subsequently, linear interpolation is
139 used in between the turning points to obtain the baseflow hydrograph. The baseflow index is obtained as the
140 ratio of the volume of water beneath the baseflow separation curve versus the total volume of water from the
141 observed hydrograph, and an average value is computed over all the observed hydrographs for a given
142 catchment. A low index is indicative of an impermeable catchment with rapid response, whereas a high value
143 suggests high storage capacity and a stable flow regime.

144 SR ($\text{m}^3 \text{s}^{-1} \text{km}^{-2}$) is computed as the mean daily flow of the river standardized by the size of its basin
145 area. It may be an important physical driver as it is an indicator of the catchment's wetness. PL (%) and PG
146 (%) are investigated for the Swedish and Austrian catchments, respectively, as lakes and glaciers are expected
147 to increase catchment storage thus affecting persistence. Lake coverage data are based on cartography and



148 available from the Swedish Water Archive (<https://www.smhi.se/>), while glacier coverage data are estimated
149 from the CORINE land cover database (<https://www.eea.europa.eu/publications/COR0-landcover>).

150 The effect of catchment altitude is also inspected using relief maps from the Shuttle Radar Topography
151 Mission (SRTM) data (<http://srtm.csi.cgiar.org/>). The data are available for the whole globe and are sampled
152 at 3 arc-seconds resolution (approximately 90 meters). Topographic information is available for all
153 catchments located at latitude lower than 60 degrees north while a 1 km resolution digital elevation model is
154 available for Austria.

155 As geological descriptors we consider the percentage of catchment area with the presence of flysch
156 (percentage of flysch, PF) and karstic formations (percentage of karst, PK) for Austrian and Slovenian
157 catchments, respectively, for which this type of information is available. A subset of Austrian catchments is
158 characterised by the dominant presence of flysch, which is known to generate a very fast flow response.
159 Karstic catchments are also known for having rapid response times and complex behaviour; e.g. initiating
160 fast preferential groundwater flow and intermittent discharge via karstic springs (Ravbar, 2013; Cervi et al.,
161 2017). Geological features are expected to be linked to persistence properties also because of geology is the
162 main control for the baseflow index across the European continent (Kuentz et al. 2017). PK (%) and PF (%)
163 are estimated from geological maps of Slovenia and Austria, respectively.

164 As climatic descriptors, the mean annual precipitation P (mm year^{-1}) and the mean annual temperature
165 T ($^{\circ}\text{C}$) are selected. Data are retrieved from the Worldclim database (<http://www.worldclim.org/>) at a spatial
166 resolution of 10 minutes of degree. We also adopt as climatic descriptor the De Martonne index (De
167 Martonne, 1926), IDM, which is given by $\text{IDM} = P/(T + 10)$, and enables classification of a region into
168 one of the following 6 climate classes, i.e., arid ($\text{IDM} \leq 5$), semi-arid ($5 < \text{IDM} \leq 10$), dry sub-humid ($10 <$
169 $\text{IDM} \leq 20$), wet sub-humid ($20 < \text{IDM} \leq 30$), humid ($30 < \text{IDM} \leq 60$) and very humid ($\text{IDM} \geq 60$).
170 Additionally, the Köppen-Geiger climatic classification (Kottek et al., 2006) of the rivers is also assessed.

171 To identify what catchment, physiographic and climatic characteristics may explain river memory we
172 attempt to regress the seasonal streamflow correlation against the physical descriptors introduced above. We



173 expect the presence of multi-collinearity among the explaining variables and therefore Principal Component
174 Analysis (PCA; Pearson, 1901; Hotelling, 1933) was applied to construct uncorrelated explanatory variables.
175 In essence, PCA is an orthonormal linear transformation of p data variables into a new coordinate system of
176 $q \leq p$ uncorrelated variables (principal components, PCs) ordered by decreasing degree of variance retained
177 when the original p variables are projected into them (Jolliffe, 2002). Therefore, the first principal axis
178 contains the greatest degree of variance in the data, while the second principal axis is the direction which
179 maximizes the variance among all directions orthogonal to the first principal axis and so on. Specifically, let
180 \mathbf{x} be a random vector with mean μ and correlation matrix Σ , then the principal component transformation of
181 \mathbf{x} is obtained as follows:

$$182 \quad \mathbf{y} = \mathbf{C}^T \mathbf{x}' \quad (1)$$

183 where \mathbf{y} is the transformed vector whose k th column is the k th principal component ($k=1, 2..p$), \mathbf{C} is the $p \times$
184 p matrix of the coefficients or loadings for each principal component and \mathbf{x}' is the standardized \mathbf{x} vector.
185 Standardization is applied in order to avoid the impact of the different variable units on selecting the direction
186 of maximum variance, when forming the PCs. The \mathbf{y} values are the scores of each observation, i.e. the
187 transformed values of each observation of the original p variables in the k th principal component direction.

188 PCA has useful descriptive properties of the underlying structure of the data. These properties can be
189 efficiently visualized in the biplot (Gabriel, 1971), which is the combined plot of the scores of the data for
190 the first two principal components along with the relative position of the p variables as vectors in the two-
191 dimensional space. Herein, the distance biplot type (Gower and Hand, 1995), which approximates the
192 Euclidean distances between the observations, is used. Variable vectors coordinates are obtained by the
193 coefficients of each variable for the first two principal components. After construction of the PCs, a linear
194 regression model is explored for the case of HFS and LFS lag-1 correlation.



195 2.3 Technical experiment: Real-time updating of the flood frequency distribution

196 In order to evaluate the usefulness of the information provided by the one-month-lag seasonal correlation for
197 HFS, we perform a real-time updating of the flood frequency distribution based on the average river flow in
198 the previous month. A similar analysis was carried out by Aguilar et al. (2017) for the Po and Danube Rivers.

199 In detail, a bi-variate meta-Gaussian probability distribution (Kelly and Krzysztofowicz, 1997;
200 Montanari and Brath, 2004) is fitted between observed peak flow in the HFS, Q_p and the average flow in the
201 pre-flood season month, Q_m . The peak flow is the dependent variable and is extracted as the peak river
202 discharge observed in the previously identified HFS. The average flow in the month preceding the HFS is
203 the explanatory variable. In the following, random variables are denoted by underscore and their outcomes
204 are written in plain form.

205 The normal quantile transform, NQT (Kelly and Krzysztofowicz, 1997), is used in order to make the
206 marginal probability distribution of dependent and explanatory variables Gaussian. This is achieved as
207 follows: a) the sample quantiles Q are sorted in increasing order e.g. $Q_{m_1}, Q_{m_2} \dots Q_{m_n}$, b) the cumulative
208 frequency FQ_{m_i} is computed via a Weibull plotting position, and c) the standard normal quantile NQ_{m_i} is
209 obtained as the inverse of the standard normal distribution for each cumulative frequency, i.e. $G^{-1}(FQ_{m_i})$.
210 Therefore, all sample quantiles are discretely mapped into the Gaussian domain. To get the inverse
211 transformation for any normal quantile NQ_{m_i} , we connect the points in the above mapping with linear
212 segments. The extreme segments are extended to allow extrapolation outside the range covered by the
213 observed sample.

214 In the Gaussian domain, a bivariate Gaussian distribution is fitted between the random explanatory
215 variable \underline{NQ}_m and the dependent variable \underline{NQ}_p assuming stationarity and ergodicity of the variables:

$$216 \quad \underline{NQ}_p(t) = \rho(\underline{NQ}_m, \underline{NQ}_p) \underline{NQ}_m(t) + N\varepsilon(t) \quad (2)$$

217 where $\rho(\underline{NQ}_m, \underline{NQ}_p)$ is the Pearson's cross correlation coefficient between \underline{NQ}_m and \underline{NQ}_p , and $N\varepsilon(t)$ is an
218 outcome of the stochastic process $\underline{N\varepsilon}$, which is independent, homoscedastic, stochastically independent of
219 \underline{NQ}_m and normally distributed with zero mean and variance $1 - \rho^2(\underline{NQ}_m, \underline{NQ}_p)$. Then, the joint bivariate



220 Gaussian probability distribution function is defined by the mean ($\mu(\underline{NQ}_m) = 0$ and $\mu(\underline{NQ}_p) = 0$), the standard
221 deviation ($\sigma(\underline{NQ}_m) = 1$ and $\sigma(\underline{NQ}_p) = 1$) of the standardized normalized series, and the Pearson's cross
222 correlation coefficient between the normalized series, $\rho(\underline{NQ}_m, \underline{NQ}_p)$. From the Gaussian bivariate probability
223 properties, it follows that for any observed $NQ_m(t)$ the probability distribution function of \underline{NQ}_p conditioned
224 on NQ_m is Gaussian, with parameters given by:

$$225 \mu(\underline{NQ}_p) = \rho(\underline{NQ}_m, \underline{NQ}_p) NQ_m \quad (3)$$

$$226 \sigma(\underline{NQ}_p) = (1 - \rho^2(\underline{NQ}_m, \underline{NQ}_p))^{0.5} \quad (4)$$

227 To derive the probability distribution of \underline{Q}_p conditioned to the observed Q_m , we apply the inverse NQT. This
228 is referred to as the updated probability distribution. We use the Extreme Value Type I distribution for the
229 peak flows and calculate the differences in the magnitude of estimated maxima for a given return period
230 between the unconditioned and the updated distribution. The latter is conditioned by the 95% sample quantile
231 of the observed mean flow in the previous month.

232 3. Data and catchments description

233 The dataset includes 224 records spanning more than 50 years of daily river flow data, mostly from non-
234 regulated streams. A few catchments are impacted by mild regulation. Among the 224 rivers, 108 are located
235 in Austria, 69 in Sweden, 31 in Slovenia, 13 in France, 2 in Spain and one in Italy. Catchment areas vary
236 significantly, the largest being the Po River basin in Italy (70 091 km²) and the smaller being the Hålabäck
237 River basin in Sweden (4.7 km²). The geographical location of the river gauge stations is shown in Fig. 1.
238 Most of the examined rivers belong to either a warm temperate (C) or a boreal/snow climate (D) with a subset
239 impacted by polar climatic conditions (E), according to the updated World Map of the Köppen-Geiger climate
240 classification (Fig. 1) based on gridded temperature and precipitation data for the period 1951-2000 (Kottek
241 et al., 2006). More specifically, the majority of French, Slovenian and approximately one third of the Swedish
242 basins belong to the warm temperate Cfb category characterized by precipitation distributed throughout the
243 year (fully humid) and warm summers. The rest of the Swedish catchments are impacted by a Dfc climatic
244 type, i.e. a snow climate, fully humid with cool summers. The Austrian catchments belonging to the region



245 impacted by the European Alps have the most complicated regime due to their topographic variability. At
246 the lowest altitudes, Cfb is the prevailing regime, but as proximity to the Alps increases, a Dfc regime
247 dominates and progressively, in the highest altitude basins, the climate becomes a polar tundra type (Et),
248 characterized primarily by the very low temperatures present. A summary of the river basins under study in
249 terms of the selected descriptors is also provided in Table 1, showing that the investigated rivers cover a wide
250 range of catchment area sizes, flow regimes and climatic conditions.

251 It is interesting to note that some of the above rivers are subject to regulation, which may alter the
252 persistence properties of river flows. On the one hand, under the assumption that river flow management
253 does not change in time, the presence of regulation does not preclude the exploitation of correlation for
254 predicting river flows in probabilistic terms. On the other hand, regulation may affect the analysis of physical
255 drivers, as it may enhance or reduce persistence in the natural river flow regime. Given that the results that
256 we herein present are derived from a large sample of catchments, we assume that they are not significantly
257 affected by the mild regulation that takes place in a few of them.

258 **4. River memory analysis for the considered case studies**

259 **4.1 Season Identification**

260 Approximately half of the 224 rivers are characterized by at least one high-flow season with medium or
261 higher significance ($\text{PAMF(HFS)} \geq 60\%$). Among them, very strong unimodal regimes ($\text{PAMF(HFS)} \geq 80$
262 $\%$) are observed in 63 rivers, the majority of which are located in Sweden. For 25% of the rivers, a high-flow
263 season of low significance is found (PAMF(HFS) between 40–60%), while for the remaining 25% the high-
264 flow distribution looks uniform along the year. Bi-modality regimes are found with low and moderate
265 significance in rivers located mostly in Austria and Sweden, but we focus here on the major high-flow season,
266 for which we inspect higher seasonal correlation against previous average flow.

267 Regarding the LFS identification, the two considered approaches (see Section 2.1) agree for 139 out of
268 224 stations but the first method, i.e. the one-month period with the lowest amount of mean monthly flow is
269 selected as being more relevant to the purpose of computing mean flow correlations.



270 4.2 Seasonal correlation

271 LFS correlation is markedly higher than the corresponding HFS correlation for lags 1–5 and its median
272 remains higher than 0 for more lags (see Fig. 2). For the case of HFS correlation, we focus only on the most
273 significant first lag, for which 73 rivers are found to have correlation significantly higher than 0 at 5 %
274 significance level. In Fig. 3, the autocorrelation of the whole monthly series is compared to the LFS
275 correlation for lag of 1 and 2 months, in order to prove that the seasonal correlation for LFS is significantly
276 higher than its counterpart computed by considering the whole year. The latter is also confirmed by the
277 Kolmogorov-Smirnov test for both LFS lags (corresponding p-values, $p_{lag1} < 2.2 \times 10^{-6}$ and $p_{lag2} < 2.2 \times 10^{-6}$
278 for the null hypothesis that the LFS correlation coefficients are not higher than the corresponding values for
279 the monthly series autocorrelation; Conover, 1971).

280 Figure 4 shows the spatial pattern of HFS and LFS streamflow correlations. It is interesting to notice
281 the emergence of spatial clustering in the correlation magnitude, which implies its dependence on different
282 spatially varying physical mechanisms. For example, for HFS, a geographical pattern emerges within France,
283 since the highest correlation coefficients are located in the northern part of the country, which is characterized
284 by oceanic climate and higher baseflow indexes.

285 5. Physical interpretation of correlation

286 To attribute the detected correlations to physical drivers, we define 6 groups of potential drivers of seasonal
287 correlation magnitude, which are: basin size, flow indexes, presence of lakes and glaciers, catchment
288 elevation, catchment geology, and hydro-climatic forcing. For some of the descriptors the information is
289 available for few countries only.

290 In what follows, we will use the term “positive (negative) impact on correlation” to imply that an
291 increasing value of the considered descriptor is associated to increasing (decreasing) correlation. For each
292 descriptor, we also report between parentheses the Spearman’s rank correlation coefficient r_s (Spearman,
293 1904) between its value and the considered (LFS or HFS) correlation, and the p-value of the null hypothesis



294 $r_s = 0$. Spearman's coefficient is adopted in view of its robustness to the presence of outliers and its capability
295 of capturing monotonic relationships of non-linear type.

296 **5.1 Catchment area – Descriptor A**

297 Figure 5 shows that there is only a weak positive impact of the catchment area (log-transformed) on
298 correlation for HFS ($r_s = 0.17$, $p = 0.01$) but a more significant positive one for LFS ($r_s = 0.27$, $p = 5.5 \times 10^{-5}$).
299 We expected a more pronounced positive impact of the catchment area. The presence of relevant scatter
300 in the plots also indicates that it is not a key determinant of correlation.

301 **5.2 Flow indexes – Descriptors BI and SR**

302 The effect of the BI and SR is shown in Fig. 6. BI (Fig. 6a) appears to be a marked positive driver for LFS
303 ($r_s = 0.6$, $p = 1.8 \times 10^{-23}$) while its effect for HFS is less clear, being weakly positive ($r_s = 0.21$, $p = 0.001$).
304 As for SR (Fig. 6b), it looks that both LFS and HFS streamflow correlations drop for increasing wetness (r_s
305 $= -0.4$, $p = 4 \times 10^{-10}$ and $r_s = -0.28$, $p = 2.8 \times 10^{-5}$ respectively).

306 **5.3 Presence of lakes and glaciers – Descriptors PL and PG**

307 Detailed information on the presence of lakes is available for the 69 Swedish catchments while areal
308 extension of glaciers is known for the 108 Austrian catchments. Figure 7 shows their impact. The impact of
309 lake area (Fig. 7a) on correlation for LFS and HFS is not significant but positive ($r_s = 0.10$, $p = 0.399$ and r_s
310 $= 0.12$, $p = 0.347$). The results for glaciers show a positive impact for LFS ($r_s = 0.28$, $p = 0.081$) but negative
311 for HFS ($r_s = -0.34$, $p = 0.032$). For a meaningful interpretation, these results should be considered in
312 conjunction with the seasonality of flows for the Austrian catchments. Low flows for the glacier-dominated
313 catchments are typically occurring in winter months, when glaciers are not contributing to the flow (Parajka
314 et al., 2009). Thus the observed result for LFS is more likely portraying the impact of low temperature (low
315 evapotranspiration) and snow accumulation, the latter generally being a slowly varying process. For HFS,
316 which is typically occurring in the summer months for the considered catchments, flows are mainly
317 determined by snowmelt which is associated to large variability and reduced persistence (Fig. 7b).



318 **5.4 Catchment elevation**

319 The areal coverage of the SRTM data is limited to 60 degrees north and 54 degrees south and therefore, data
320 for the northern part of the Swedish catchments are not available. The rest of the rivers are divided in three
321 regions based on proximity: Region I including the central and eastern part of the Alps and encompassing
322 Austrian, Slovenian and Italian catchments; Region II showing the western part of the Alps and encompassing
323 French and Spanish territory; and Region III including the southern part of Sweden. Figure 8 shows elevation
324 maps along with the location of gauge stations and magnitude of correlations. Elevation seems to enhance
325 LFS correlation which is more evident in the mountainous Region I (Fig. 8). For HFS correlation there is not
326 a prevailing pattern.

327 In the case of Austrian catchments, a 1 km resolution digital model is also used to extract information
328 on elevation. Figure 9 confirms that there is a positive correlation pattern emerging with elevation for LFS.
329 Based on local climatological information, it can be concluded that the spatial pattern for LFS correlation is
330 reflective of the timing and strength of seasonality of the low flows in Austria, where dry months occur in
331 lowlands during the summer due to increased evapotranspiration and in the mountains during winter (mostly
332 February) due to snow accumulation which is characterised by stronger seasonality compared to the lowlands
333 flow regime (Parajka et al., 2016; see Fig. 1). Concerning HFS in the same region, high flows are significantly
334 impacted by the seasonality of extreme precipitation (Parajka et al., 2010), which is highly variable, with the
335 exception of the rivers where high flows are generated by snowmelt. Therefore, a spatially consistent pattern
336 does not clearly emerge.

337

338 **5.5 Catchment geology – Descriptors PK and PF**

339 Two different geological behaviours are identified which may impact river correlation. We first focus on 21
340 Slovenian catchments (out of 31) where more than 50 % of the basin area is characterised by the presence of
341 karstic aquifers (percentage of karstic areas $PK \geq 50\%$). Figure 10 shows boxplots of the estimated lag-1



342 correlation coefficient for both HFS and LFS against rivers where $PK < 50\%$. It is clear that there is a
343 significant decrease in correlation where karstic areas dominate for both for HFS and LFS.

344 In a second analysis, we focus on Austrian catchments and investigate the relationship between
345 correlation and percentage of Flysch coverage, PF. Figure 11 shows that there is not a prevailing pattern in
346 either case ($r_s = 0.13$, $p = 0.6$ for LFS and $r_s = -0.19$, $p = 0.446$ for HFS).

347 5.6 Atmospheric forcing – Descriptors P and T

348 Figure 12 shows the lag-1 HFS and LFS correlations against estimates of the annual precipitation P and
349 annual mean temperature T as well as the De Martonne index IDM. LFS correlation looks more sensitive
350 than HFS to the above climatic indices, showing a decrease with increasing temperature and also a decrease
351 with increasing precipitation ($r_s = -0.44$, $p = 3.1 \times 10^{-12}$ for P and $r_s = -0.57$, $p = 1.8 \times 10^{-20}$ for T). HFS
352 correlation looks scarcely sensitive to these variables ($r_s =$
353 -0.17 , $p = 0.011$ for P and $r_s = 0.08$, $p = 0.208$ for T). The IDM (Fig. 12 c) shows a mild decrease of both
354 LFS ($r_s = -0.06$, $p = 0.368$) and HFS correlation with increasing IDM ($r_s = -0.17$, $p = 0.01$), while for the
355 latter there seems to be a clearer trend (lower correlation with higher IDM) in very humid areas (dark blue
356 points in Fig. 12c).

357

358 5.7 Physical drivers of high correlation

359 To gain further insights into the results we select the 20 catchments having the highest streamflow seasonal
360 correlation coefficients for both HFS and LFS periods in order to investigate their physical characteristics in
361 relation to the remaining set of rivers. Table 2 summarizes statistics for selected descriptors in order to
362 identify dominant behaviours. We also compare the number of rivers with distinctive features, i.e. lakes N_L
363 (number of rivers with lakes), glaciers N_G (number of river with glaciers), flysch N_F (number of rivers with
364 flysch formations) and karst N_K (number of rivers with karstic areas) for the highest correlation group with



365 those obtained from 1000 randomly sampled 20-catchment groups from the whole set of considered
366 catchments to assess whether higher correlation implies distinctive features.

367 By focusing on HFS, one can notice that the catchments with higher seasonal correlation are
368 characterised by larger catchment area, higher baseflow index and temperature with respect to the remaining
369 catchments, and lower specific runoff, precipitation and wetness. Presence of lake, glaciers, karstic and
370 Flysch areas do not appear significantly effective at a 5 % significance level. More robust considerations can
371 be drawn for the LFS: higher seasonal correlation is found for larger catchments with higher baseflow index
372 and lower specific runoff, precipitation and wetness. Decreasing temperature is strongly associated with
373 higher correlation for the LFS. The presence of lakes plays a significant role both for lag-1 and lag-2
374 correlations with the latter being also significantly influenced by presence of glaciers.

375 **6. Principal component analysis of the predictors and linear regression**

376 We attempt to fit a linear regression model to relate correlation to physical drivers, in order to support
377 correlation estimation for ungauged catchments. To avoid the impact of multicollinearity in the regression
378 while additionally summarize river information, we apply a PCA analysis (see Section 2.2). Although
379 correlation effects are efficiently dealt with via the PCA, we avoid including highly correlated variables in
380 the analysis. For example, the De Martonne Index, Precipitation and SR are mutually highly correlated (all
381 Pearson's cross-correlations are higher than 0.6) and therefore we only consider the SR in the PCA because
382 it shows a more robust linear relationship with correlation magnitude. We select A , BI , SR and T as the
383 variables to be considered in the PCA. A log transformation is applied on the basin area to reduce impact of
384 outliers. Table 3 shows the coefficients estimated for each component (the loadings) and the explained
385 variance. The first principal component is primarily a measure of BI ; the second principal component majorly
386 accounts for T and the third principal component accounts for A . There is an evident geographical pattern
387 emerging by the visualization of countries in the biplot (Fig. 13). Slovenian rivers cluster towards the
388 direction of increasing SR and T , whereas Swedish rivers towards the opposite direction of increasing BI and



389 decreasing T . Austrian rivers, which are the majority, are the most diverse. The first two components together
390 explain the 70 % of the total variability in the data.

391 Naturally, the statistical behaviour of the indexes reflects the known local controls for certain rivers.
392 For example, the observed lowest BI in Slovenia is consistent with the presence of karstic formations for the
393 majority of the Slovenian rivers, as also is the higher BI in Sweden and Austria, which is related to the
394 presence of lakes and glaciers in both countries.

395 In the case of HFS, all the examined linear models (combinations of $\ln A$, SR, BI, P , T , IDM predictors)
396 failed in explaining the streamflow correlation magnitude. On the contrary, the linear regression model
397 performs fairly well in explaining the correlation for LFS, with an adjusted R^2 value of 0.58 and an F-test
398 returning a p-value $< 2.2 \times 10^{-16}$. The coefficients for the first three PCs are found significantly different from
399 zero at a 0.1 % significance level and are included in the regression (see Table 4). The highest coefficient is
400 obtained for the first PC, which mostly accounts for BI importance. Diagnostic plots from linear regression
401 for LFS are shown in Fig. 14. There is no clear violation of the homoscedasticity assumption in linear
402 regression, apart from the presence of a limited number of outliers. There is a certain departure from
403 normality in the lower tail of the residuals, which relates to the fact that the model performs better in the area
404 of higher seasonal streamflow correlations and overestimates the lower correlations.

405

406 **7. Real-time updating of the flood frequency distribution for selected rivers**

407 We apply the technical experiment to two rivers with significant lag-1 streamflow correlation for HFS and
408 assess the difference in the estimated flood magnitudes. The first river is the Oise River (55 years of daily
409 flow values) at Sempigny in France with correlation $\rho = 0.54$, which is the 3rd largest lag-1 correlation for
410 the HFS in our dataset. The second river is the Torsebro River at Helge in Sweden (53 years of daily flow
411 values). Its lag-1 correlation coefficient for the HFS equals 0.46 which ranks 9th among the rivers. The
412 Torsebro River has a catchment area of 3665 km² with lake coverage of 5.4 %, while the Oise River
413 catchment is slightly larger (4320 km²).



414 A visual inspection of the residuals plots for both rivers is also performed (Fig. 15a, b) in order to
415 evaluate the assumption of homoscedasticity of the residuals of the regression model given by Eq. (2). The
416 residuals do not show any apparent trend and therefore the Gaussian linear model is accepted. Figure 15 (c,
417 d) shows the conditioned and unconditioned probability distributions of peak flows in the Gaussian domain.
418 As expected from Eq. (3) and (4), the variance of the updated (conditioned) distribution decreases while the
419 mean value increases.

420 After application of the inverse NQT the conditioned peak flows are modelled through the EV1
421 distribution and compared to the unconditioned (observed) peak flows. The corresponding Gumbel
422 probability plots for conditioned and unconditioned distributions are shown in Fig. 15 (e, f) for the two rivers.
423 For the return period of 200 years, the updated distribution shows a 6 % increase in the flood magnitude for
424 the Oise River ($307.7 \text{ m}^3 \text{ s}^{-1}$ to $326.44 \text{ m}^3 \text{ s}^{-1}$) and a 10 % increase for the Torsebro River ($298.07 \text{ m}^3 \text{ s}^{-1}$ to
425 $329.22 \text{ m}^3 \text{ s}^{-1}$).

426 8. Discussion and Conclusions

427 The methodology presented herein aims to progress our physical understanding of seasonal river flow
428 persistence for the sake of exploiting the related information to improve probabilistic prediction of high and
429 low flows. The correlation of average flow in the previous months with LFS flow and HFS peak flow was
430 found to be relevant, with the former prevailing on the latter. This result was expected since the LFS
431 correlation refers to average flow while the HFS correlation is related to rapidly occurring events. We also
432 aim to investigate physical drivers for correlation. Therefore, a thorough investigation of the geophysical and
433 climatological features of the considered catchments was carried out.

434 We found that increasing basin area and baseflow index are associated with increasing seasonal
435 streamflow correlation. Within this respect, Mudelsee (2007), Hirpa et al. (2010) and Szolgayova et al.
436 (2014a) also found positive dependencies of long-term persistence on basin area, Markonis et al. (2018)
437 found a positive impact too but for larger spatial scales ($> 2 \times 10^4 \text{ km}^2$), while Gudmunsson et al. (2011)
438 found basin area to have negligible to no impact to the low-frequency components of runoff. Our results



439 additionally point out that catchment storage induces mild positive correlation, not only for low discharges
440 which are directly governed by base flow, but also for high flows.

441 Previous studies also pointed out that correlation increases for groundwater-dominated regimes (Yossef
442 et al., 2013; Dijk et al., 2013; Svensson, 2016) and slower catchment response times (Bierkens and van Beek,
443 2009), which concurs with the impact of baseflow index found herein as well as with the observed impact of
444 fast responding karst areas. The latter findings are also in agreement with our conclusion that correlation
445 decreases for increasing rapidity of river flow formation, which for instance occurs in the presence of karstic
446 areas and wet soils, which explains why persistence decreases with high specific runoff; as also confirmed
447 by other studies (Gudmundsson et al., 2011; Szolgayova et al., 2014).

448 Other contributions also reported higher streamflow persistence in drier conditions, either relating to
449 lower specific runoff or mean areal precipitation estimates (Szolgayova et al., 2014; Markonis et al., 2018).
450 It was postulated that this is due to wet catchments showing increased short-term variability compared to
451 drier catchments (Szolgayova et al., 2014) and having a faster response to rainfall due to saturated soil. A
452 similar conclusion has been reached by other previous studies reporting that low humidity catchments are
453 more sensitive to inter-annual rainfall variability (Harman et al., 2011), therefore leading to enhanced
454 persistence. Yet, these studies refer to generally humid regions and cannot be extrapolated to more arid
455 climates. A related conclusion is proposed by Seneviratne et al. (2006) who found the highest soil moisture
456 memory for intermediate soil wetness. There results do not contrast with our findings, which refer to a wide
457 range of climatic conditions.

458 We also confirm the role of lakes in determining higher catchment storage and therefore positive
459 correlations for the LFS, which has been reported for annual persistence in a few sites (Zhang et al., 2012).

460 The effect of snow cover for lag-1 LFS correlation is also revealed by the Austrian catchments. The
461 mountainous rivers, directly affected by the process of snow accumulation, exhibit winter LFS and higher
462 correlation than the rivers in the lowlands, which are more prone to drying out due to evapotranspiration in
463 the hotter summer months. The inspection of elevation data confirmed the role of high altitudes in increasing



464 LFS correlation, which is likely related to storage effects due to snow accumulation and gradual melting. In
465 this respect, Kuentz et al. (2017) found that topography exerts dominant controls over the flow regime in the
466 larger European region, controlling the flashiness of flow, and being a particularly important driver for other
467 low flow signatures too. In fact, topography may affect the flow regime directly, through flow routing, but
468 also indirectly, because of orographic effects in precipitation and hydroclimatic processes affected by
469 elevation (e.g. snowmelt and evapotranspiration).

470 Regarding atmospheric forcing, we find LFS correlation to be negatively correlated to mean areal
471 temperature and annual precipitation. The former result may be explained considering that increased
472 evapotranspiration (higher temperature) is expected to dry out LFS flows while snow coverage (lower
473 temperature) was found to be associated to higher LFS correlation. An apparently different conclusion was
474 drawn by Szolgayova et al. (2014a) and Gudmundsson et al. (2011), who reported increasing persistence
475 with increasing mean temperature postulating that snow-dominated flow regimes smooth out interannual
476 fluctuations. Yet, it should be noted that they refer to interannual variability while we refer here to seasonal
477 correlation and therefore to shorter time scales, which imply a different dynamic of snow accumulation and
478 snowmelt; latitude may also play a relevant role in this, since in southern Europe the complete ablation of
479 snow can occur more than once during the cold season, and sublimation may account for 20–30 % of the
480 annual snowfall (Herrero and Polo, 2016), decreasing the amount of snowmelt and impacting LFS flows in
481 the summer season.

482 Snowmelt mechanisms are found to increase predictive skill during low-flow periods in some other
483 studies (Bierkens and van Beek, 2009; Mahanama et al., 2011; Dijk et al., 2013). However, in the glacier-
484 dominated regime of western Alpine and central Austrian catchments this is not expected to be a relevant
485 driver of higher correlation, since low flow is occurring in the winter months. Yet the mountainous, glacier-
486 dominated rivers still show increased LFS correlation compared to rivers in the lowlands, which agrees well
487 with other studies that have found less uncertainty in the rainfall-runoff modelling in this regime owing to



488 the greater seasonality of the runoff process and the decreased impact of rainfall compared to the rainfall-
489 dominated regime of the lowlands (e.g Parajka et al., 2016).

490 Although the considerable uncertainty of areal precipitation estimates should be acknowledged, the
491 contribution of annual precipitation interestingly complements the negative effect of increasing specific
492 runoff –which is highly correlated to P estimates– on the correlation magnitude for both LFS and HFS. This
493 outcome confirms that catchments receiving significant amount of rainfall do show less correlation than drier
494 regimes.

495 We conclude that our results are essentially in agreement with the relevant literature and point out the
496 possibility to exploit river memory within a data assimilation context to reduce uncertainty in the prediction
497 of future high and low flows. The opportunity of exploiting correlation is not affected by the presence of
498 regulation, provided the management of river flow does not change in time. Therefore, river memory is an
499 interesting option to inspect opportunities for improving the prediction of water-related natural hazards.

500 **Data and Code availability**

501 The data and code used in this study may be made available to the readers upon request to the corresponding
502 author.

503 **Competing interests**

504 The authors declare that they have no conflict of interest.

505 **Acknowledgements**

506 The present work was (partially) developed within the framework of the Panta Rhei Research Initiative of
507 the International Association of Hydrological Sciences (IAHS). Part of the results were elaborated in the
508 Switch-On Virtual Water Science Laboratory that was developed in the context of the SWITCH-ON (Sharing
509 Water-related Information to Tackle Changes in the Hydrosphere – for Operational Needs) project, funded
510 by the European Union Seventh Framework Programme (FP7/2007-2013) under grant agreement no. 603587.



- 511 N. Bezak gratefully acknowledges funding by the Slovenian Research Agency (grants J2-7322 and P2-0180).
- 512 M. Bermúdez gratefully acknowledges financial support from the Spanish Regional Government of
- 513 Galicia, Postdoctoral Grant Program 2014.

514 References

- 515 Aguilar, C., Montanari, A., Polo, M.-J., 2017. Real-time updating of the flood frequency distribution through
516 data assimilation. *Hydrol. Earth Syst. Sci.* 21, 3687–3700. <https://doi.org/10.5194/hess-21-3687-2017>
- 517 Bierkens, M.F.P., van Beek, L.P.H., 2009. Seasonal Predictability of European Discharge: NAO and
518 Hydrological Response Time. *Journal of Hydrometeorology* 10, 953–968.
519 <https://doi.org/10.1175/2009JHM1034.1>
- 520 Cervi, F., Blöschl, G., Corsini, A., Borgatti, L., Montanari, A., 2017. Perennial springs provide information
521 to predict low flows in mountain basins. *Hydrological Sciences Journal* 62, 2469–2481.
522 <https://doi.org/10.1080/02626667.2017.1393541>
- 523 Chiew, F.H.S., Zhou, S.L., McMahon, T.A., 2003. Use of seasonal streamflow forecasts in water resources
524 management. *Journal of Hydrology* 270, 135–144. [https://doi.org/10.1016/S0022-1694\(02\)00292-5](https://doi.org/10.1016/S0022-1694(02)00292-5)
- 525 Conover, W.J., 1971. *Practical Nonparametric Statistics*. New York: John Wiley and Sons. Inc.
- 526 Cunderlik, J.M., Ouada, T.B., Bobée, B., 2004. Determination of flood seasonality from hydrological
527 records/Détermination de la saisonnalité des crues à partir de séries hydrologiques. *Hydrological*
528 *Sciences Journal* 49. <https://doi.org/10.1623/hysj.49.3.511.54351>
- 529 De Martonne, E.M., 1926. L'indice d'aridité. *Bulletin de l'Association de géographes français* 3, 3–5.
530 <https://doi.org/10.3406/bagf.1926.6321>
- 531 Dijk, A.I., Peña-Arancibia, J.L., Wood, E.F., Sheffield, J., Beck, H.E., 2013. Global analysis of seasonal
532 streamflow predictability using an ensemble prediction system and observations from 6192 small
533 catchments worldwide. *Water Resources Research* 49, 2729–2746.
534 <https://doi.org/10.1002/wrcr.20251>
- 535 Dimitriadis, P., Koutsoyiannis, D., Tzouka, K., 2016. Predictability in dice motion: how does it differ from
536 hydro-meteorological processes? *Hydrological Sciences Journal* 61, 1611–1622.
537 <https://doi.org/10.1080/02626667.2015.1034128>
- 538 Gabriel, K.R., 1971. The biplot graphic display of matrices with application to principal component analysis.
539 *Biometrika* 58, 453–467. <https://doi.org/10.1093/biomet/58.3.453>
- 540 Gower, J.C., Hand, D.J., 1995. *Biplots*. CRC Press.
- 541 Gudmundsson, L., Tallaksen, L.M., Stahl, K., Fleig, A.K., 2011. Low-frequency variability of European
542 runoff. *Hydrology and Earth System Sciences* 15, 2853–2869. [https://doi.org/10.5194/hess-15-2853-](https://doi.org/10.5194/hess-15-2853-2011)
543 [2011](https://doi.org/10.5194/hess-15-2853-2011)
- 544 Gustard, A., Demuth, S., others, 2009. *Manual on low-flow estimation and prediction*. Opera.
- 545 Harman, C.J., Troch, P.A., Sivapalan, M., 2011. Functional model of water balance variability at the
546 catchment scale: 2. Elasticity of fast and slow runoff components to precipitation change in the
547 continental United States. *Water Resources Research* 47. <https://doi.org/10.1029/2010WR009656>
- 548 Herrero, J., Polo, M.J. 2016. Evapostublimation from the snow in the Mediterranean mountains of Sierra
549 Nevada (Spain). *The Cryosphere*, 10, 2981–2998, <https://doi.org/10.5194/tc-10-2981-2016>
- 550 Hirpa, F.A., Gebremichael, M., Over, T.M., 2010. River flow fluctuation analysis: Effect of watershed area.
551 *Water Resources Research* 46. <https://doi.org/10.1029/2009WR009000>
- 552 Hurst, H.E., 1951. Long-term storage capacity of reservoirs. *Trans. Amer. Soc. Civil Eng.* 116, 770–808.
- 553 Jolliffe, I., 2002. *Principal component analysis*. Wiley Online Library.
554 <https://doi.org/10.1002/9781118445112.stat06472>



- 555 Kelly, K.S., Krzysztofowicz, R., 1997. A bivariate meta-Gaussian density for use in hydrology. *Stochastic*
556 *Hydrology and hydraulics* 11, 17–31. <https://doi.org/10.1007/BF02428423>
- 557 Kottek, M., Grieser, J., Beck, C., Rudolf, B., Rubel, F., 2006. World Map of the Köppen-Geiger climate
558 classification updated. *Meteorologische Zeitschrift* 259–263. [https://doi.org/10.1127/0941-](https://doi.org/10.1127/0941-2948/2006/0130)
559 [2948/2006/0130](https://doi.org/10.1127/0941-2948/2006/0130)
- 560 Koutsoyiannis, D., 2011. Hurst-Kolmogorov Dynamics and Uncertainty. *JAWRA Journal of the American*
561 *Water Resources Association* 47, 481–495. <https://doi.org/10.1111/j.1752-1688.2011.00543.x>
- 562 Koutsoyiannis, D., Yao, H., Georgakakos, A., 2008. Medium-range flow prediction for the Nile: a
563 comparison of stochastic and deterministic methods/Prévision du débit du Nil à moyen terme: une
564 comparaison de méthodes stochastiques et déterministes. *Hydrological Sciences Journal* 53, 142–164.
565 <https://doi.org/10.1623/hysj.53.1.142>
- 566 Kuentz, A., Arheimer, B., Hundecha, Y. and Wagener, T., 2017. Understanding hydrologic variability across
567 Europe through catchment classification. *Hydrology and Earth System Sciences*, 21(6), p.2863–2879,
568 <https://doi.org/10.5194/hess-21-2863-2017>.
- 569 Lee, D., Ward, P., Block, P., 2015. Defining high-flow seasons using temporal streamflow patterns from a
570 global model. *Hydrology and Earth System Sciences* 19, 4689–4705. [https://doi.org/10.5194/hess-19-](https://doi.org/10.5194/hess-19-4689-2015)
571 [4689-2015](https://doi.org/10.5194/hess-19-4689-2015)
- 572 Mahanama, S., Livneh, B., Koster, R., Lettenmaier, D., Reichle, R., 2011. Soil Moisture, Snow, and Seasonal
573 Streamflow Forecasts in the United States. *J. Hydrometeor.* 13, 189–203.
574 <https://doi.org/10.1175/JHM-D-11-046.1>
- 575 Markonis, Y., Moustakis, Y., Nasika, C., Sychova, P., Dimitriadis, P., Hanel, M., Máca, P., Papalexiou, S.M.,
576 2018. Global estimation of long-term persistence in annual river runoff. *Advances in Water Resources*
577 113, 1–12. <https://doi.org/10.1016/j.advwatres.2018.01.003>
- 578 Montanari, A., 2012. Hydrology of the Po River: looking for changing patterns in river discharge. *Hydrology*
579 *and Earth System Sciences* 16, 3739–3747. <https://doi.org/10.5194/hess-16-3739-2012>
- 580 Montanari, A., Brath, A., 2004. A stochastic approach for assessing the uncertainty of rainfall-runoff
581 simulations. *Water Resources Research* 40. <https://doi.org/10.1029/2003WR002540>
- 582 Mudelsee, M., 2007. Long memory of rivers from spatial aggregation. *Water Resources Research* 43.
583 <https://doi.org/10.1029/2006WR005721>
- 584 O’Connell, P.E., Koutsoyiannis, D., Lins, H.F., Markonis, Y., Montanari, A., Cohn, T., 2016. The scientific
585 legacy of Harold Edwin Hurst (1880–1978). *Hydrological Sciences Journal* 61, 1571–1590.
586 <https://doi.org/10.1080/02626667.2015.1125998>
- 587 Parajka, J., Blaschke, A.P., Blöschl, G., Haslinger, K., Hepp, G., Laaha, G., Schöner, W., Trautvetter, H.,
588 Viglione, A., Zessner, M., 2016. Uncertainty contributions to low-flow projections in Austria. *Hydrol.*
589 *Earth Syst. Sci.* 20, 2085–2101. <https://doi.org/10.5194/hess-20-2085-2016>
- 590 Parajka, J., Kohnová, S., Bálint, G., Barbuc, M., Borga, M., Claps, P., Cheval, S., Dumitrescu, A., Gaume,
591 E., Hlavčová, K., others, 2010. Seasonal characteristics of flood regimes across the Alpine–
592 Carpathian range. *Journal of hydrology* 394, 78–89. <https://doi.org/10.1016/j.jhydrol.2010.05.015>
- 593 Parajka, J., Kohnová, S., Merz, R., Szolgay, J., Hlavčová, K., Blöschl, G., 2009. Comparative analysis of the
594 seasonality of hydrological characteristics in Slovakia and Austria/Analyse comparative de la
595 saisonnalité de caractéristiques hydrologiques en Slovaquie et en Autriche. *Hydrological Sciences*
596 *Journal* 54, 456–473. <https://doi.org/10.1623/hysj.54.3.456>
- 597 Piechota, T.C., Chiew, F.H., Dracup, J.A. and McMahon, T.A., 2001. Development of exceedance
598 probability streamflow forecast. *Journal of Hydrologic Engineering*, 6(1), pp.20–28.
599 [https://doi.org/10.1061/\(ASCE\)1084-0699\(2001\)6:1\(20\)](https://doi.org/10.1061/(ASCE)1084-0699(2001)6:1(20))
- 600 Ravbar, N., 2013. Variability of groundwater flow and transport processes in karst under different hydrologic
601 conditions/Spremenljivost Pretakanja Voda in Prenosa Snovi V Krasu ob Razlicnih Hidroloških
602 Pogojih. *Acta Carsologica* 42, 327. <http://dx.doi.org/10.3986/ac.v42i2.644>
- 603 Seneviratne, S.I., Koster, R.D., Guo, Z., Dirmeyer, P.A., Kowalczyk, E., Lawrence, D., Liu, P., Mocko, D.,
604 Lu, C.-H., Oleson, K.W., others, 2006. Soil moisture memory in AGCM simulations: analysis of



- 605 global land–atmosphere coupling experiment (GLACE) data. *Journal of Hydrometeorology* 7, 1090–
 606 1112. <https://doi.org/10.1175/JHM533.1>
- 607 Spearman, C., 1904. The Proof and Measurement of Association between Two Things. *The American Journal*
 608 *of Psychology* 15, 72–101. <https://doi.org/10.2307/1412159>
- 609 Svensson, C., 2016. Seasonal river flow forecasts for the United Kingdom using persistence and historical
 610 analogues. *Hydrological Sciences Journal* 61, 19–35. <https://doi.org/10.1080/02626667.2014.992788>
- 611 Szolgayova, E., Laaha, G., Blöschl, G., Bucher, C., 2014. Factors influencing long range dependence in
 612 streamflow of European rivers. *Hydrological Processes* 28, 1573–1586.
 613 <https://doi.org/10.1002/hyp.9694>
- 614 Wang, Q.J., Robertson, D.E., Chiew, F.H.S., 2009. A Bayesian joint probability modeling approach for
 615 seasonal forecasting of streamflows at multiple sites. *Water Resources Research* 45.
 616 <https://doi.org/10.1029/2008WR007355>
- 617 Yossef, N.C., Winsemius, H., Weerts, A., Beek, R., Bierkens, M.F., 2013. Skill of a global seasonal
 618 streamflow forecasting system, relative roles of initial conditions and meteorological forcing. *Water*
 619 *Resources Research* 49, 4687–4699. <http://dx.doi.org/10.1002/wrcr.20350>
- 620 Zhang, Q., Zhou, Y., Singh, V.P., Chen, X., 2012. The influence of dam and lakes on the Yangtze River
 621 streamflow: long-range correlation and complexity analyses. *Hydrological Processes* 26, 436–444.
 622 <http://dx.doi.org/10.1002/hyp.8148>
- 623

624 Tables

625 **Table 1** Summary statistics of the river descriptors. Summary statistics for PL, PG and PF variables are computed
 626 only for the subset of catchments with positive values (the total number of catchments is also reported in brackets).
 627 PK is used as a categorical variable (PK is either higher or lower than 50 % of catchment area), therefore sample
 628 statistics are not computed in this case, but the number of stations with $PK \geq 50\%$ is reported as ‘positive’ presence
 629 of karst.

Descriptor (Units)	A (km ²)	BI (–)	SR (m ³ s ⁻¹ km ⁻²)	PL (%)	PG (%)	PF (%)	PK (–)	P (mm year ⁻¹)	T (°C)	IDM (–)
Min	4.7	0.29	0.004	0.5	0.1	0.3	–	444	–1.8	29.41
Max	70091	0.99	0.088	19.5	56.5	100	–	1500	13.7	153.40
Standard deviation	5904.3	0.14	0.018	4.04	15.54	32.56	–	288.22	3.59	24.53
Sample size	224	224	224	69 [69]	39 [108]	18 [108]	21 [31]	224	224	224

630

631

632

633

634



635 **Table 2** Differences in the mean values between the descriptors of the 20-highest correlation river group for HFS and
 636 LFS vs the remaining rivers (204). N_L , N_G , N_F and N_K columns contain the absolute number of rivers in the higher
 637 correlation group with the specific descriptor (presence of lake, glacier, flysch and karst) with * denoting
 638 significance at 5 % significance level (two-sided test) and brackets containing the mean value from the 1000
 639 resampled 20-catchment subsets.

Descriptor (Units)	A (km ²)	BI (-)	SR (m ³ s ⁻¹ km ⁻²)	N_L (-)	N_G (-)	N_F (-)	N_K (-)	P (mm year ⁻¹)	T (°C)	IDM (-)
HFS lag1	+38.7 %	+9.6 %	-36.5 %	5 [6]	5 [3]	1 [2]	1 [2]	-6.7 %	+11.7 %	-11.3 %
LFS lag1	+358 %	+20.2 %	-47.3 %	17* [6]	3 [3]	0 [2]	0 [2]	-37.9 %	-80 %	-17.3 %
LFS lag2	+139.7 %	+18.9 %	-40.8 %	12* [6]	7* [3]	0 [2]	0 [2]	-26.5 %	-64.2 %	-8.8 %

640

641 **Table 3** Loadings of the three Principal Components for $\ln A$, SR , BI and T . The explained variance of each PC is
 642 denoted in parenthesis.

Predictor variables	PC1 (42.5 %)	PC2 (28.2 %)	PC3 (17 %)	PC4 (12.2 %)
$\ln A$	-0.486	-0.427	0.748	0.145
SR	0.48	0.483	0.652	-0.332
BI	-0.619	0.262	-0.11	-0.731
T	0.385	-0.718	-0.04	-0.577

643

644 **Table 4** Summary of Linear Regression results for the LFS model. *** indicate a 0.1 % significance level.

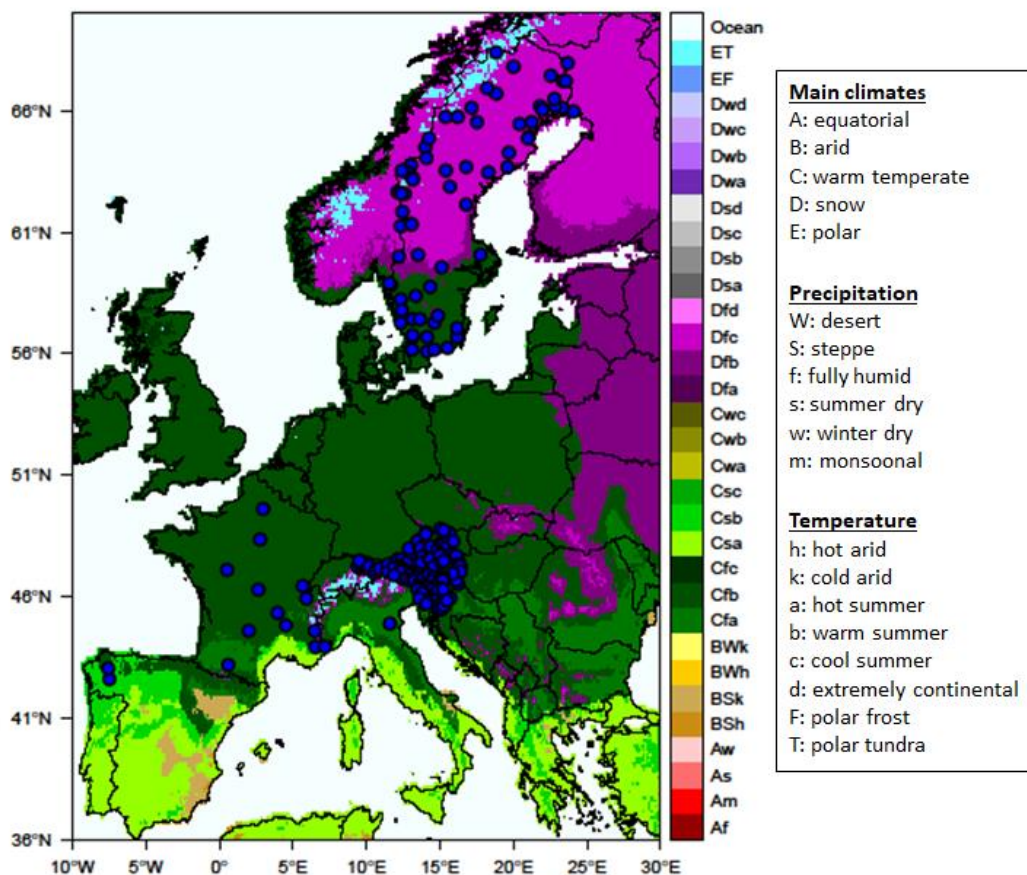
Predictor variables	Estimate	Standard Error	t value	Pr(> t)	Adjusted R ²	F-statistic
intercept	0.659407	0.008557	77.065	< 2 × 10 ⁻¹⁶ ***	0.5834	104.2
PC1	-0.110632	0.006577	-16.820	< 2 × 10 ⁻¹⁶ ***		p-value:
PC2	0.031761	0.008070	3.936	0.000111***		< 2.2 × 10 ⁻¹⁶
PC3	-0.038999	0.010388	-3.754	0.000223***		

645

646

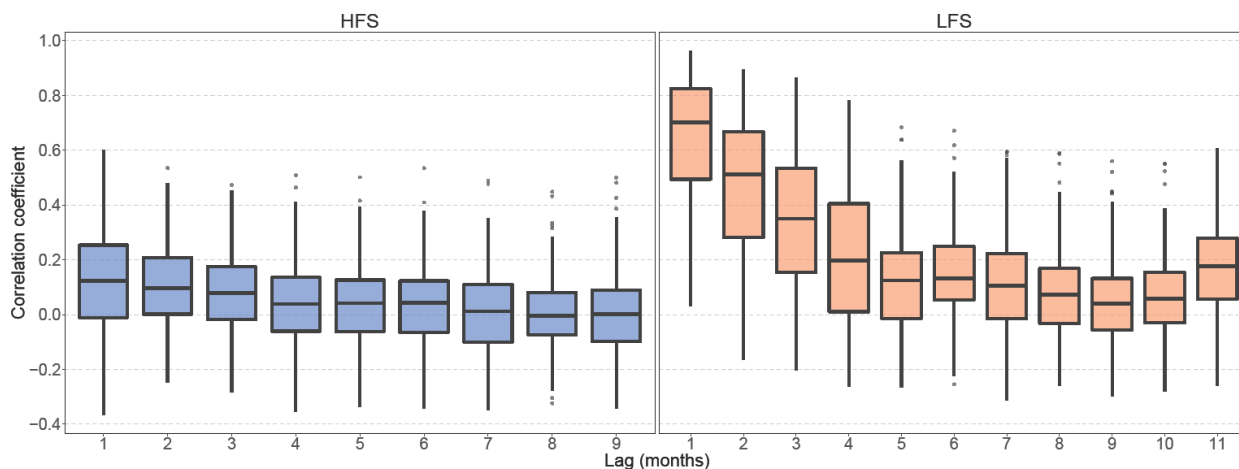


647 **Figures**



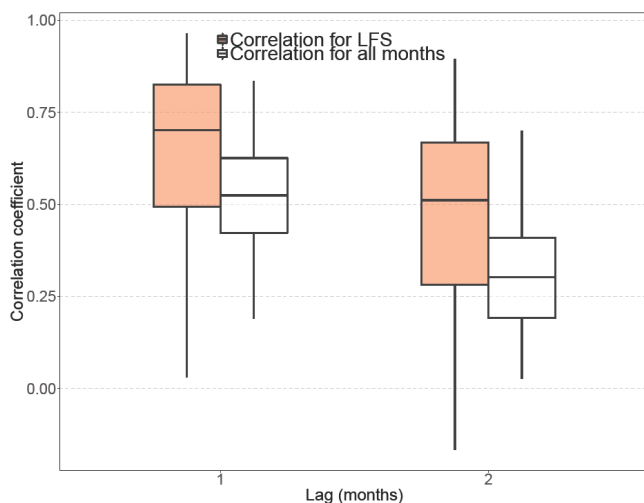
648

649 **Figure 1.** Updated Köppen-Geiger climatic map for period 1951–2000 (Kottek et al., 2006) showing the location of
 650 the 224 river gauge stations.

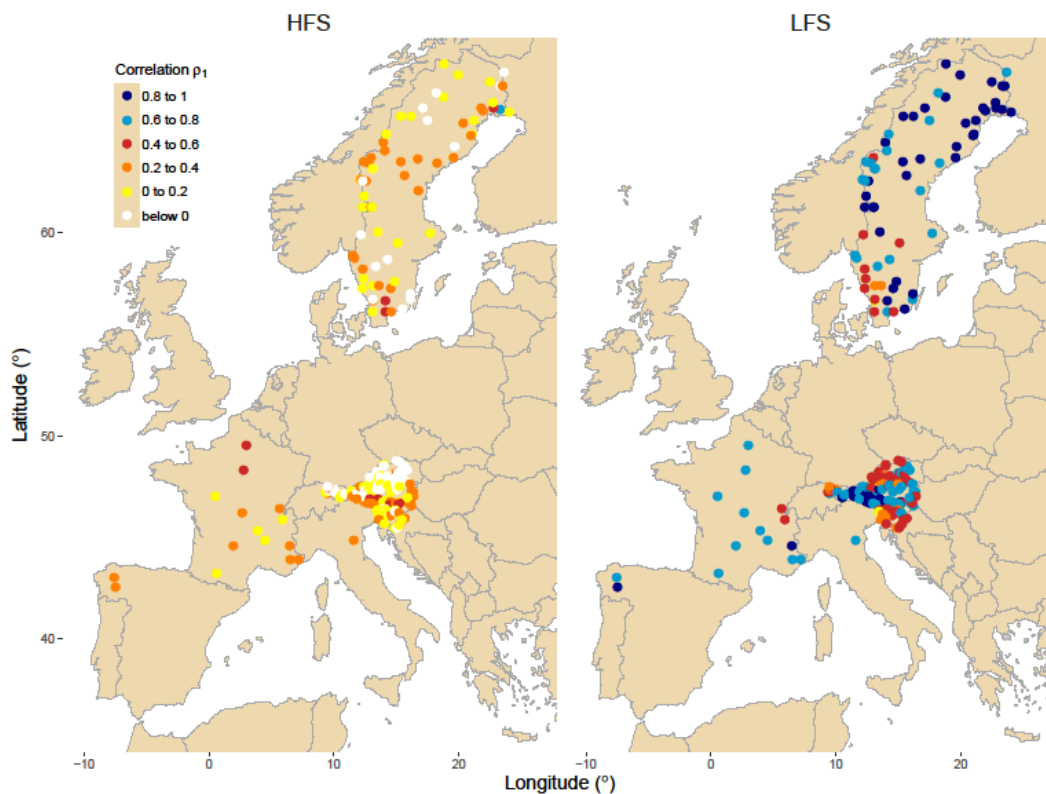


651
 652 **Figure 2.** Boxplots of seasonal correlation coefficient against lag time for HFS (left panel) and LFS (right panel)
 653 analysis. The lower and upper ends of the box represent the 1st and 3rd quartiles, respectively, and the whiskers extend
 654 to the most extreme value within 1.5 IQR (interquartile range) from the box ends; outliers are plotted as filled circles.

655

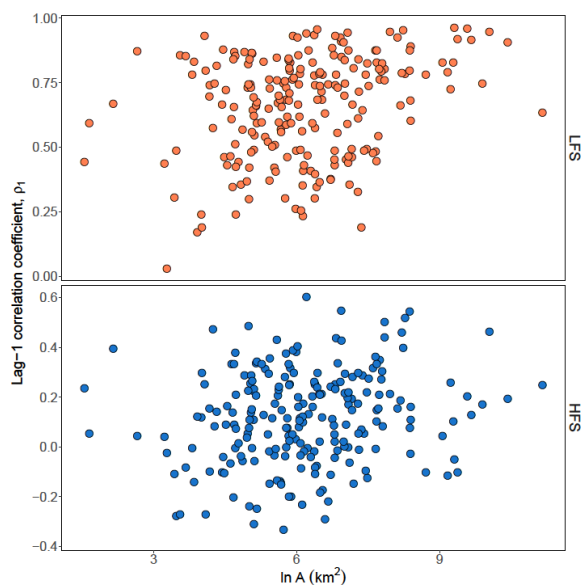


656
 657 **Figure 3.** Boxplots of lag-1 and lag-2 correlation coefficients for LFS analysis (orange) and the whole monthly series
 658 (white). The lower and upper ends of the box represent the 1st and 3rd quartiles, respectively, and the whiskers extend
 659 to the most extreme value within 1.5 IQR (interquartile range) from the box ends.



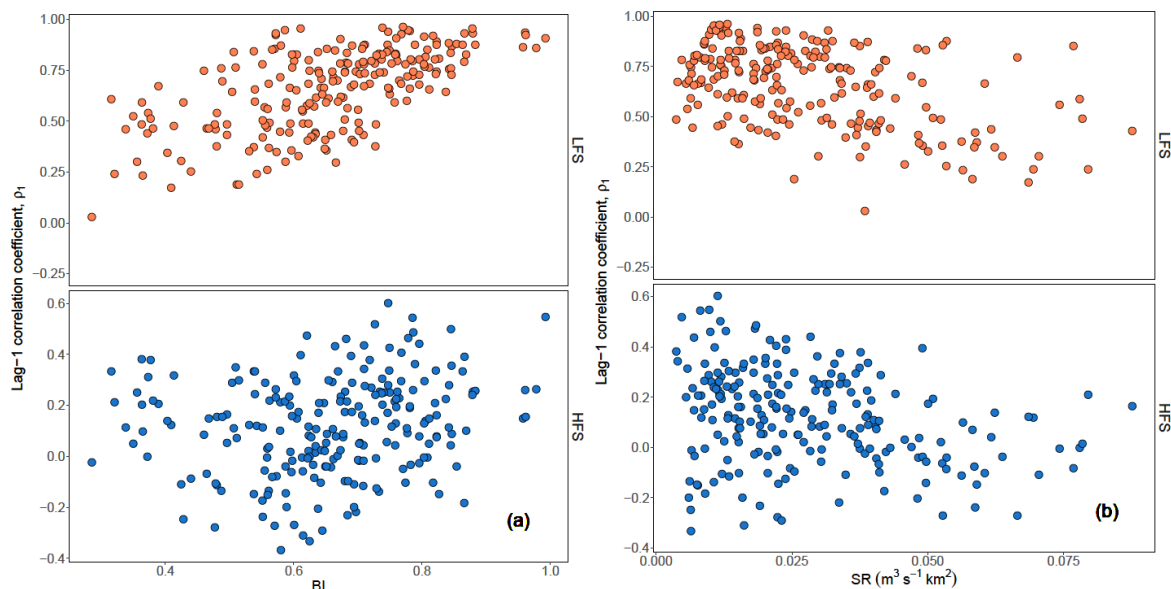
660

661 **Figure 4.** Spatial distribution of the lag-1 correlation coefficients for HFS (left) and LFS (right) analysis. Legend
 662 shows the color assigned to each class of correlation for the data.



663
 664
 665

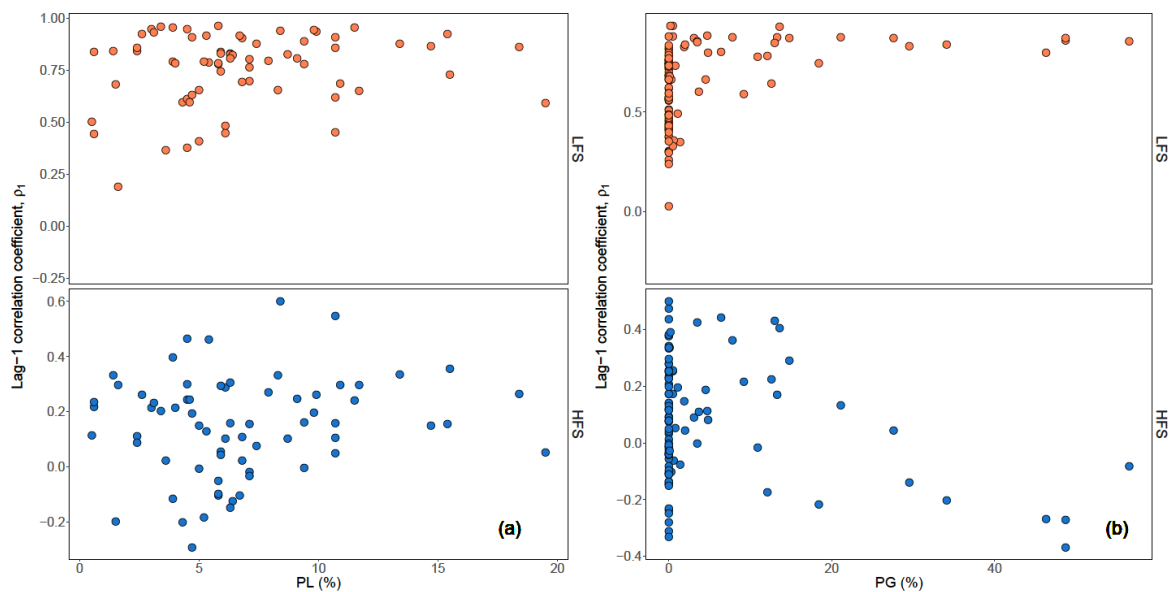
Figure 5. Scatterplots of lag-1 HFS (bottom panel) and LFS (top) streamflow correlation versus the natural logarithm
 of basin area $\ln A$.



666

667 **Figure 6.** Scatterplots of lag-1 HFS (bottom panels) and LFS streamflow correlation (top panels) versus baseflow
 668 index BI (a) and specific runoff SR (b).

669

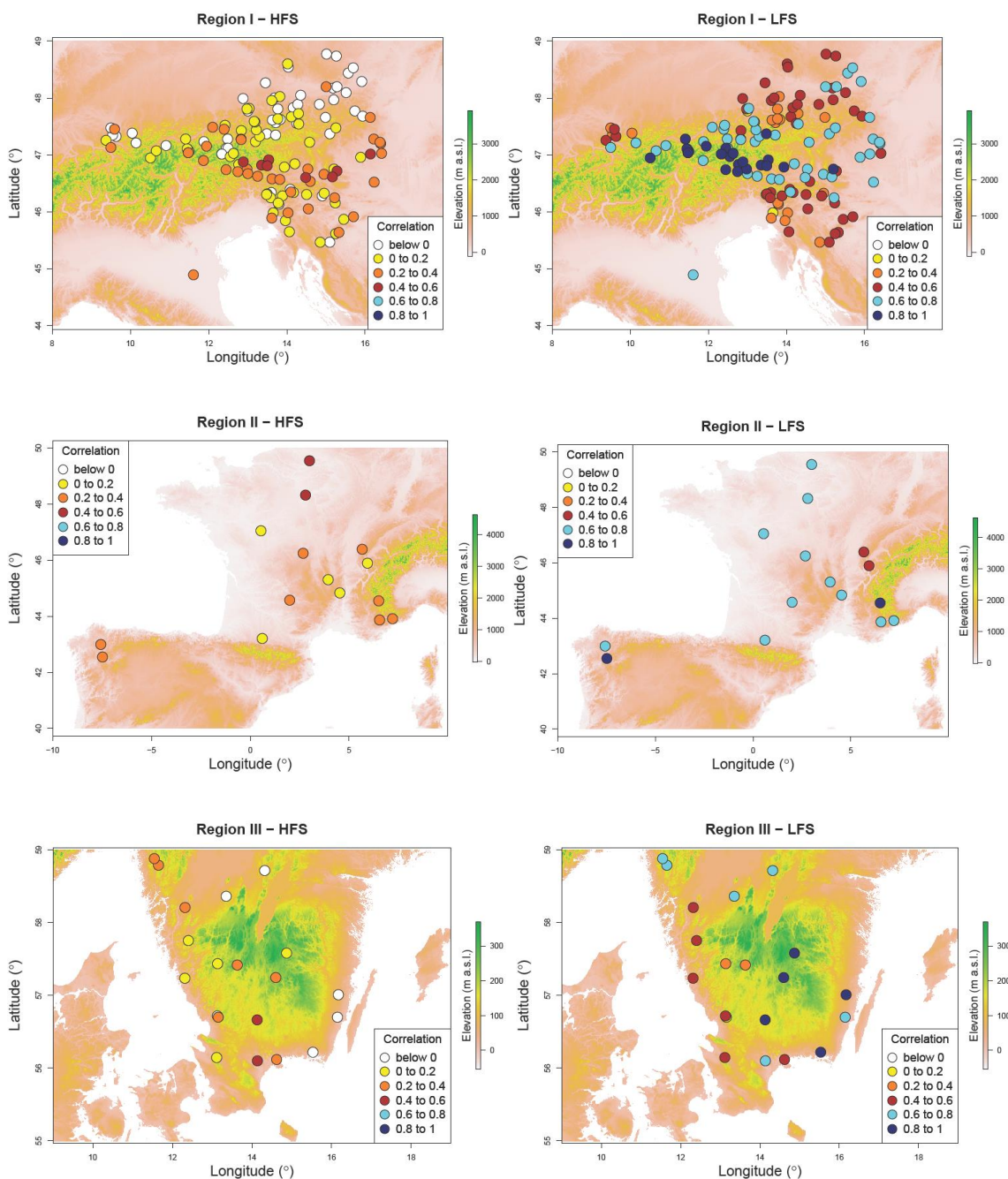


670

671 **Figure 7.** Scatterplots of lag-1 HFS (bottom) and LFS (top) streamflow correlations versus percentage of lakes PL of
 672 the Swedish catchments (a) and percentage of glaciers PG of the Austrian catchments (b).

673

674



675

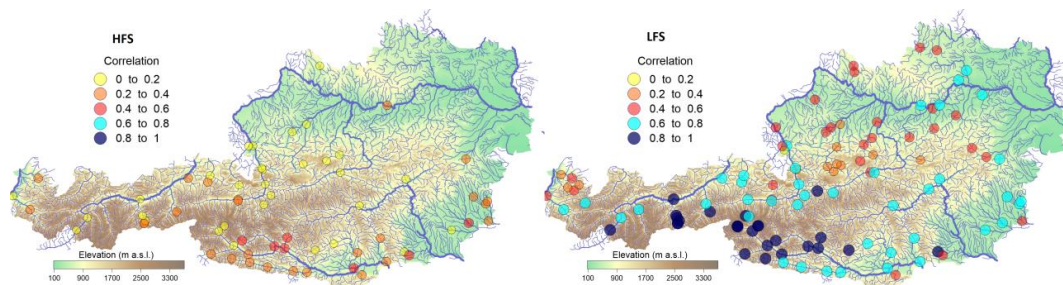
676

677

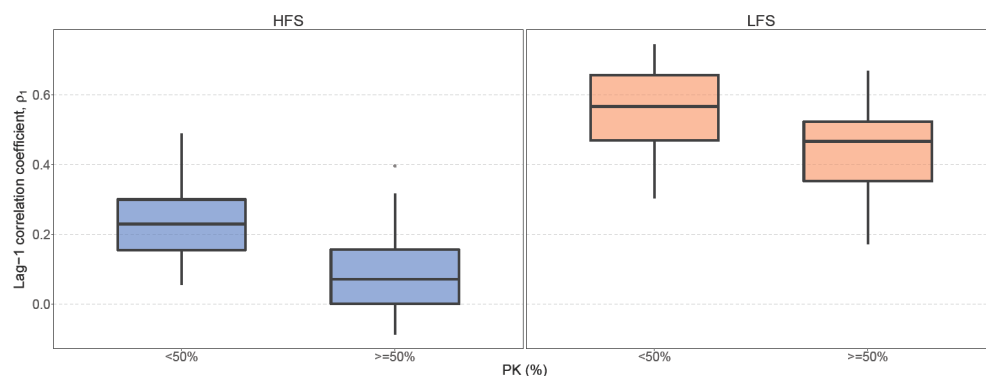
678

679

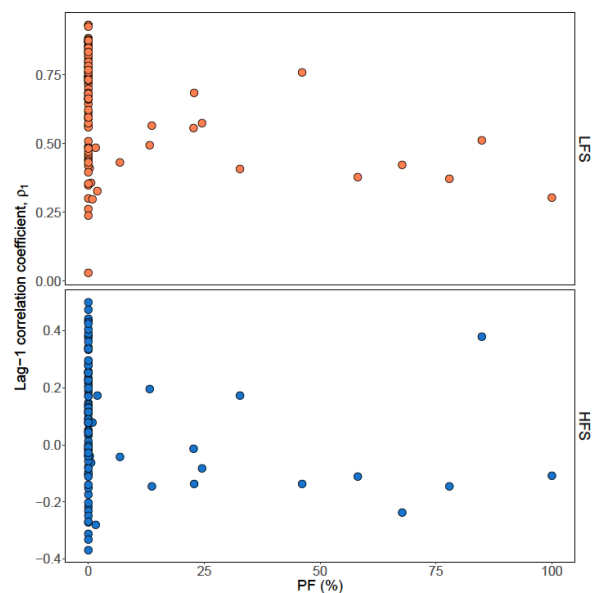
Figure 8. Relief maps from SRTM elevation data for the HFS and LFS lag-1 correlations of the rivers. Note that elevation scale is different for each region. Legend shows the colour assigned to each class of correlation for the data.



680
 681 **Figure 9.** Digital elevation model of the Austrian river network depicting the spatial distribution of lag-1 positive
 682 correlation for HFS (left) and lag-1 positive correlation for LFS (right). Legend shows the colour assigned to each
 683 class of correlation for the data.

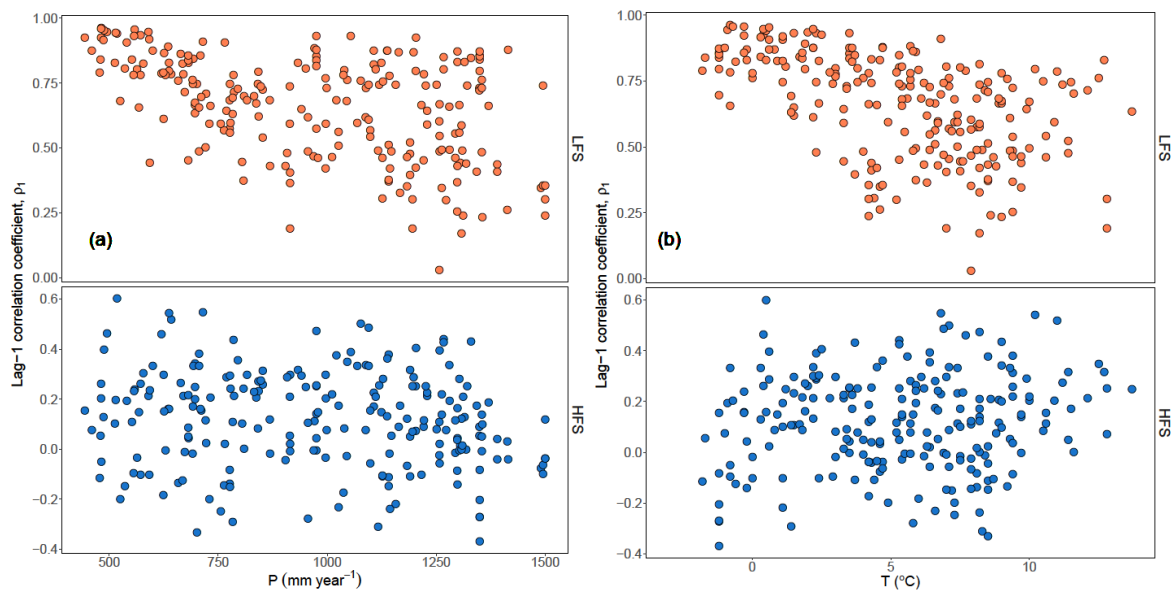


684
 685 **Figure 10.** Boxplots of lag-1 correlation for Slovenian rivers with more than 50% presence of karstic formations PK
 686 and rivers with no or less presence for HFS analysis (left) and LFS analysis (right). The lower and upper ends of the
 687 box represent the 1st and 3rd quartiles, respectively, and the whiskers extend to the most extreme value within 1.5
 688 IQR (interquartile range) from the box ends.

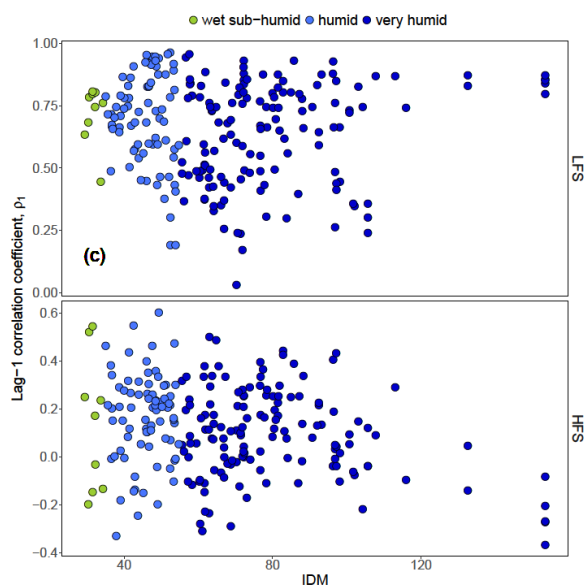


689
 690 **Figure 11.** Scatterplots of lag-1 correlation vs percentage of flysch area coverage PF for HFS (bottom) and LFS (top)
 691 analysis for the Austrian catchments.

692



693

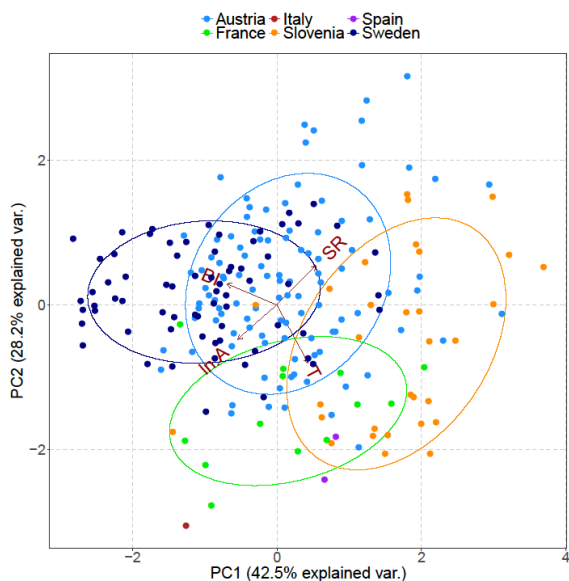


694

695

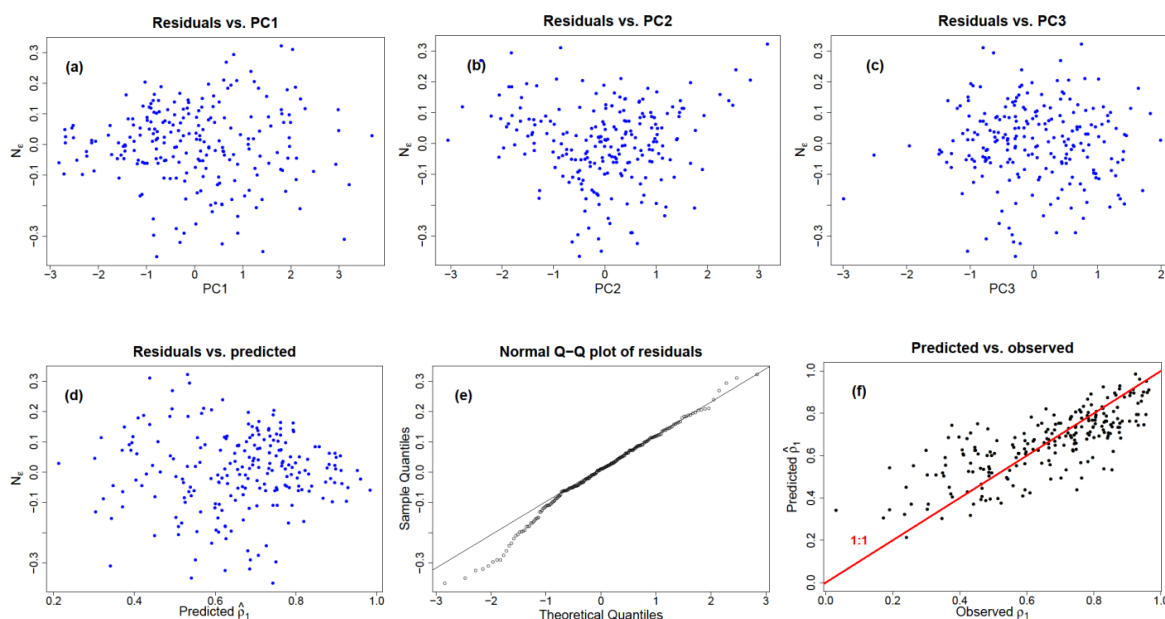
696

Figure 12. Scatterplots of lag-1 HFS and LFS correlation versus annual precipitation P (a), mean annual temperature T (b), and Index De Martonne IDM (c).



697

698 **Figure 13.** Principal component distance biplot showing the principal component scores on the first two principal
 699 axes along with the vectors (brown arrows) representing the coefficients of the baseflow index BI, specific runoff SR,
 700 natural logarithm of basin area $\ln A$ and mean annual temperature T variables when projected on the principal axes.
 701 Scores for the rivers are plotted in different colors corresponding to each country of origin and 68% normal
 702 probability contour plots are plotted for the countries.



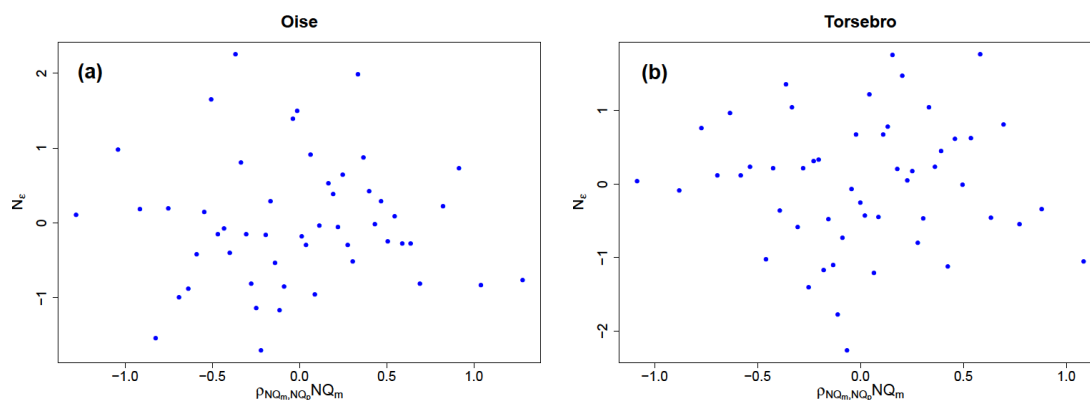
703

704

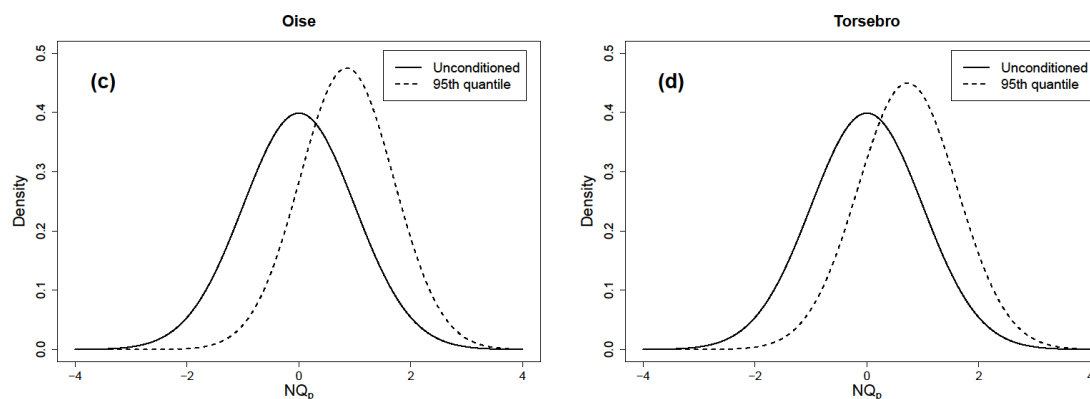
705 **Figure 14.** Diagnostic plots of linear regression for the LFS model. Residuals versus the first (a), the second (b) and
 706 the third principal component (c) and the predicted values (d). Normal Q-Q plot of the residuals (e). Plot of the
 707 predicted values from linear regression vs the observed ones; red line is the diagonal line 1:1 (f).



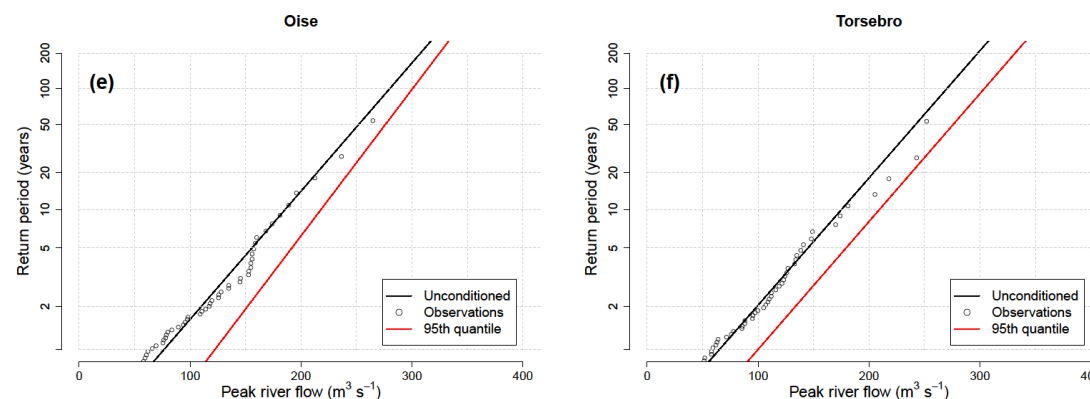
708



709



710



711 **Figure 15.** Conditioning the flood frequency distribution for the Oise River and the Torsebro River. Plots of the
 712 residuals of the linear regression given by Eq. (2) for the Oise River (a) and the Torsebro River (b). Probability
 713 distribution of the unconditional normalized peak flows NQ_p (solid line) and the normalized peak flows NQ_p
 714 conditioned to the occurrence of the 95% quantile (dotted line) for the Oise River (c) and the Torsebro River (d).
 715 Gumbel probability plots of the return period vs the unconditional peak flows Q_p (black line) and the peak flows Q_p
 716 conditioned to the occurrence of the 95 % quantile (red line) for the Oise River (e) and the Torsebro River (f).